

STAGED REFINED RESTORATION FRAMEWORK OF ARCHITECTURAL HERITAGE DAMAGED EAVES TILE OF REPEATING PATTERNS

Jiale Zhang, Hanbin Luo, Shiping Liu
Huazhong University of Science and Technology, Wuhan, China

Abstract

Eaves tiles, as significant artefacts of Chinese cultural heritage, are valued for their intricate inscriptions, animal motifs, and repeating patterns, which offer critical insights into historic architecture, art, and ideology. However, environmental exposure and human activity degradation often obscure their repetitive and symmetrical structures, complicating direct analysis. The author proposes a staged restoration framework combining geometric feature extraction and image inpainting to address this. Integrating the Hough transform with the Hierarchical Density-Based Spatial Clustering of Applications with Noise (HDBSCAN) algorithm, our method infers missing regions from rubbings without relying on intact sections of the same tile, ensuring global consistency. A geometric property-targeted database enables feature matching and candidate selection for restoration. Our approach outperforms baselines, achieving an average FID of 27.25, DISTS of 0.2135, L0SSIM of 0.8513, and inpainting duration of $5.59e^{-2}$ seconds. By integrating rough-fine geometric extraction, pattern line fitting, and structure-guided inpainting, the framework generates diverse restoration candidates with high structural and aesthetic fidelity, serving as a robust tool for cultural heritage research.

© 2025 The Authors. Published by the International Association for Automation and Robotics in Construction (IAARC) and Diamond Congress Ltd.

Peer-review under responsibility of the scientific committee of the Creative Construction Conference 2025.

Keywords: architectural heritage ornament, eaves tile, geometric feature, image inpainting, repeating pattern, rubbing image.

1. Introduction

Architectural heritage retains significant value for studying structural, stylistic, and decorative features despite the shift from traditional masonry to modern materials[1]. In China, eaves tiles—initially functional components for waterproofing and drainage—evolved into ornamental elements on palaces and ceremonial structures, embodying cultural symbolism through motifs, inscriptions, and relief work. Their artistic value lies in axis-symmetrical or center-centered continuous surface embellishments[2]—pictures (mostly animals), patterns (mostly cloud veins), and characters (mostly lucky words)—can be interpreted as accurate repetition (repetition of the same visual elements in the same way) and alternating repetition (two or more elements repeated in a fixed pattern), reflecting societal and cultural evolution. However, clay-based tile is particularly vulnerable to environmental degradation. Physical weathering (water erosion, freeze-thaw cycles, wind abrasion) and chemical processes (salt migration, oxidation, atmospheric gas reactions) cause surface deterioration[3]. Biological factors, including microbial and fungal activity in humid conditions, further accelerate degradation via acidolysis. This progressive damage compromises the structural integrity and aesthetic value (Figure 1(a)). Traditionally, artisans repair damaged areas by copying the remaining surface patterns for ornaments with symmetrical and repeatable characteristics. However, the above global damage occurred in eaves tiles, making it challenging to identify the original texture from a copied eaves tile.

Eaves tile belongs to bas-relief with a lack of complex spatial characteristics. Compressing flat structures vertically can be used to analyze and reconstruct their damage damage[4, 5]. The rubbing can[6] serve as an intermediary to reproduce the texture of the ornament's surface, making it helpful in identifying pattern defects and restoration details, as shown in Figure 1(b) and (c). Based on this, the author developed a new methodology called Staged Refined Restoration Framework of Architectural Heritage Damaged Eaves Tiles with Repeating Patterns. This approach combines the Hough transform with the Hierarchical Density-Based Spatial Clustering of Applications with Noise algorithm (HT_HDBSCAN), with the rubbing image about the damaged eaves tile as the input, to infer the missing area without referencing the existing area in the same tile. In addition, a geometric property-targeted database is built in advance to provide an index of the numerous typical pattern units and their geometric attributes that can be used to match extracted features to identify the final candidates. Tested on numerous rubbings, the framework outperforms another in-painting network in aesthetic and statistical metrics while preserving the eaves tile's structural authenticity and style.

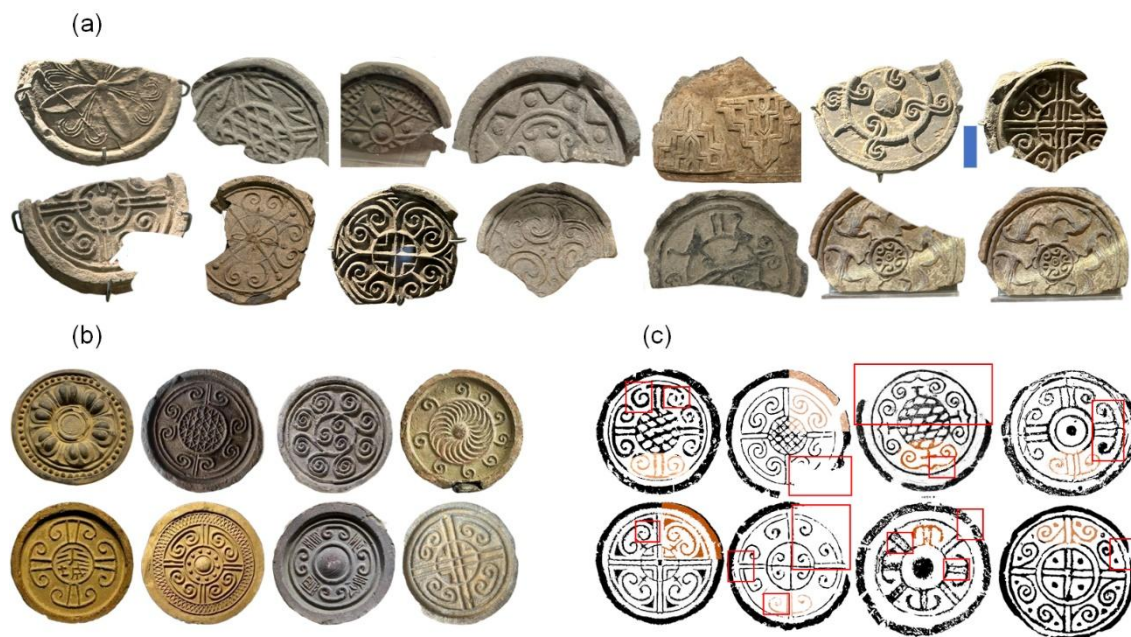


Figure 1 Illustrative legend. a) eaves tiles with global damage; b) eaves tiles engraved with repeating patterns; c) eaves tile's rubbings, orange section is a repeating unit and red box is a damaged part

2. Related work

2.1. Current restores methods toward to heritage architectural ornament

Restoration of cultural heritage buildings is a complex and vital process [7]. Unfortunately, due to the erosion of original parts, a lack of experience, and limited knowledge among artisans, it is challenging to restore handly [8]. Historical atlases, museum collections, and architectural records serve as references for restoration, providing crucial data on the era, typology, and function. Restoration methods depend on available resources—comparative replication is employed when analogous artefacts exist, utilizing techniques such as contour tracing and pattern rubbing. Missing elements may be supplemented through extrapolation based on content and craftsmanship analysis, ensuring minimal visual disparity and historical authenticity. Besides, researchers have attempted to use cutting-edge technologies to infer ornament defects, such as high dynamic range imaging, panoramic imaging, photogrammetry techniques, laser scanning, etc. Since these studies are primarily entity-targeted to infer defects, physical environments inevitably interfered with them.

2.2. Image inpainting technology

Inpainting aims to recover the original information about missing areas of images that blur, raindrops, fog, colour distortion, and occlusion have degraded. Advancements in computer vision have made it increasingly necessary to inspect images for defects[9]. Furthermore, people are becoming more aware

of restoring damaged objects such as murals, porcelain, teeth, and cultural relics[10]. There are three general categories of image inpainting research: pixel-based[11], exemplar-based[12], and global region-based[13]. The inpainting of architectural ornament images is challenging[14] because the ornaments have intricate and professional colour patterns, varied lines, and so on. Besides, the insufficient existence of heritage architectural ornament images cannot satisfy the requirement of an image inpainting algorithm that requires a large amount of training data. Thus, the standard algorithms cannot identify the relationship between existing and missing components.

3. Method

Based on rubbings, the author develops a new in-painting framework for repairing damaged tiles with repetitive patterns. A geometry-targeted database is initially built from the perspective of geometric relationships between tiles' decorative units. HT_HDBSCAN is used to extract the feature of the disappearing end of the unit once the defective parts have been identified. Database searches and defect location features are essential. It can be achieved by focusing on the endpoint of a decorative curve. A "cluster" of point sets resembling the central object will be created to extract the geometric characteristics of defective parts more precisely for further traverse and match.

3.1. Geometric property-targeted database

This study develops a 2D-geometric property-targeted database to systematically catalogue the pattern unit of eaves tile's rubbings, transforming fragmented units into an organized, retrievable system. Using over 500 rubbings, the study leverages unit repeatability and geometric relationships—both between units and their main line—to establish a structured database for further matching.

Tile decoration is usually detached from their concrete and intuitive images, full of vigorous freehand brushwork, such as sunflower patterns, cloud patterns, lotus patterns, gluttonous patterns, vortex patterns, and animal and plant patterns. Eaves tile has two elements: "inner circle" and "outer circle". The inner circle is a single-line, double-line, or three-line circular ring. This article defines the outermost circle as the "mainline," as shown in Figure 4. The decorative pattern comprises three basic elements: dots, lines, and surfaces, which create the unique beauty of tile decoration. Dots are relatively minor elements, and this article will not focus on them. Line plays a crucial role in tile decoration. The outline is always the most significant feature of its form. The repeated unit of tile decoration is constructed by various lines such as straight lines, curves, wavy lines, radiation lines, and S-shaped lines, visually presenting a harmonious sense of rhythm and rhythm.

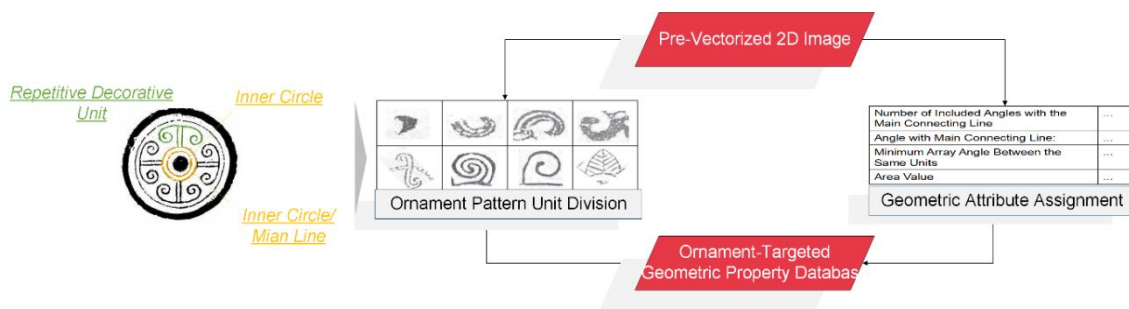


Figure 2 Establishment process of the geometric property-targeted database

Plenty of rubbings of eaves tiles with repetitive patterns, which contain the graphical and geometric information associated, are unified for subsequent extraction. The repetitive decorative unit is precisely described and numbered in the transitional database, preceding 'Geometric property-targeted database.'. Then, the geometric relationships between the units and units with the main line are defined and extracted, such as the number of angles with the main line, an angle with the main line, a minimum array angle between the same units, and a value for the area of each unit.

3.2. Interrupted-line Detection

The Hough Transform detects lines by converting image-space curves into parameter-space peaks, transforming global features into localized parametric representations. Preprocessing includes: 1) RGB-

to-grayscale conversion, 2) Gaussian denoising, 3) Sobel-based edge detection. In Hough space, edge points vote for (r, θ) candidates, with intensity peaks identifying dominant boundaries. Threshold-based local maxima extraction yields precise corners, validated through sunflower pattern analysis.

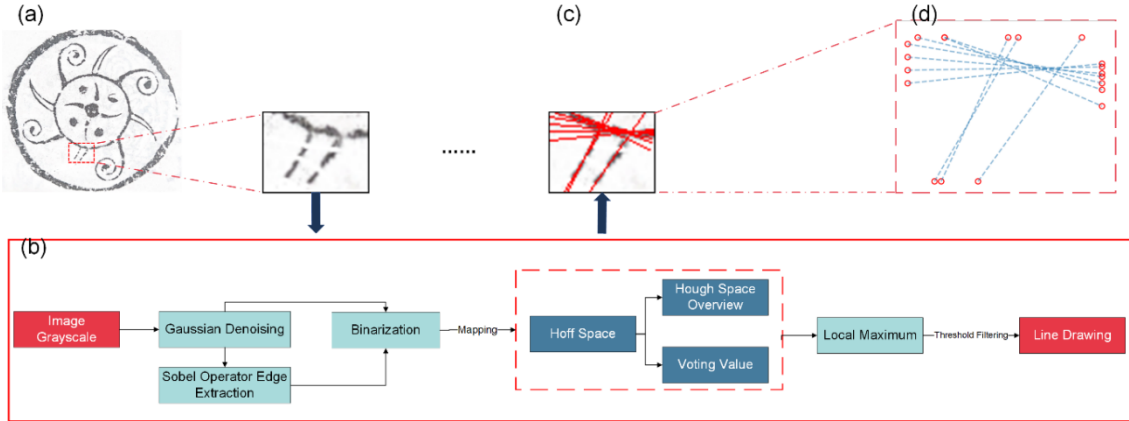


Figure 3 Schematic diagram of Hough transform line extraction and endpoint distribution

Damaged lines can be identified using central straight lines. Line endpoints can determine straight-line distribution and position, clusters can determine the distribution of central line endpoints, and the cluster's number is adaptively estimated, as shown in Figure 3(d).

3.3. Geometric features extraction

After the Hough Transform, a Hierarchical Density-Based Spatial Clustering of Applications with Noise (HDBSCAN) algorithm can cluster the line groups, which combines Density-Based Spatial Clustering of Applications with Noise and Hierarchical Clustering algorithms.

4.3.1 Spatial Transformation through Sparsity

Defective texture lines exhibited sparsity and discontinuity. Unlike multi-link clustering, single-link clustering is highly sensitive to noise, risking misclustering when noisy points bridge distinct clusters. To mitigate this, the author uses a novel distance metric to identify low-density points by comparing sampling point distances to ensure sample distances in dense regions remain robust. It utilises two key concepts: ① Core distance, distance from point x and its nearest neighbour sample point, expressed as $core\ distance_k(x)$, in Equ. (1); ② Reachability distance, Maximum between the core distances of points a and b and or their Euclidean distance, expressed as $d_{mreach-k}(a, b)$, in Equ. (2). The choice of K influences spatial transformation—larger K values increase core and mutual reachability distances due to sparser point distributions in low-density regions.

$$core\ distance_k(x) = d(x, N_k(x)) \quad (1)$$

$$d_{mreach-k}(a, b) = \max\{core\ distance_k(a), core\ distance_k(b), d(a, b)\} \quad (2)$$

4.3.2 Minimum spanning tree generation using Prim's algorithm

A. Establishing a measure of pixel similarity

Space-transformed graphs consist of two sets: \mathbf{V} and \mathbf{E} . Vertex set \mathbf{V} represents a finite non-empty set of vertex pairs, and edge set \mathbf{E} describes the edge pairs in a vertex set \mathbf{V} . Euclidean length represents the distance between adjacent pixels in the connected network $\mathbf{G} = (\mathbf{V}, \mathbf{E})$. The weight of a spanning tree is determined by its edge's length between adjacent pixels in a spatially transformed image. A similarity measure E is the difference between their spectral measures in Equ.3.

$$E = \left\{ \varepsilon_k (A_i, A_j) = g_{ij} \cdot d(A_i, A_j) \right\}, g_{ij} = \begin{cases} 0, & A_i \text{ and } A_j \text{ is disconnected} \\ 1, & A_i \text{ and } A_j \text{ is connected} \end{cases} \quad (3)$$

g_{ij} represents connectivity, $d(A_i, A_j)$ is the similarity function, $d(A_i, A_j) = \sqrt{(A_i - A_j)}$.

B. Construction of a weighted undirected graph

An undirected weighted graph $G = (A, E, W)$ is defined to represent an image. In this graph, $A = \{A_i(x_k, y_j), i = 1, 2, 3, \dots, n; k = 1, 2, 3, \dots, p; j = 1, 2, 3, \dots, m\}$ represents the set of nodes, n represents the number of pixels, and p and m represent the number of rows and columns in the image. $E = \{e_{kj}, k = 1, 2, 3, \dots, p; j = 1, 2, 3, \dots, m\}, e_{kj} = \{e_1, e_2, e_3, e_4\}$ represents the edges connecting the $(k, j)_{th}$ node to its four neighbouring nodes: above, below, to the left, and the right. Calculate pixel weights based on the Euclidean distance between colour vectors. The similarity between pixels decreases as the distance increases, resulting in lower weight values. A weighted matrix, $W = \{w_{kj}, k = 1, 2, 3, \dots, p; j = 1, 2, 3, \dots, m\}, w_{kj} = \{r, g, b, A_{up}, d_{up}, A_{down}, d_{down}, A_{left}, d_{left}, A_{right}, d_{right}\}$, is established, the index number A_{up}, d_{up} of the node on the pixel, and the distance between the pixel and the node, respectively. Other components also follow a similar pattern, as depicted in Figure 4(a). The connections between all endpoints form a phase-free graph, as illustrated in Figure 4(b).

C. Prim's algorithm based Minimum Spanning Tree Construction (MST)

Initializing the node set $T(A) = \{A_i\}$ and edge set $T(E) = \{\}$ and finding the minimum weight edge (A_k, A_g) in the edge set E require any $A_k \in T(A), A_g \in T(A)$. The found minimum weight edge is added to $T(E)$, and A_g is added to $T(A)$. Cycle through this step until all nodes are added to the selected point set. Then, the minimum spanning tree is created by subtracting one edge from each node and adding the resulting edge set $T(E)$. Edge weights, such as ϖ_a between points ① and ②, are computed, and the minimum among alternatives (e.g., ϖ_b and ϖ_v for points ③ and ④) is selected to expand the MST; the final MST only retain the necessary edges, as shown in Figure 4(c).

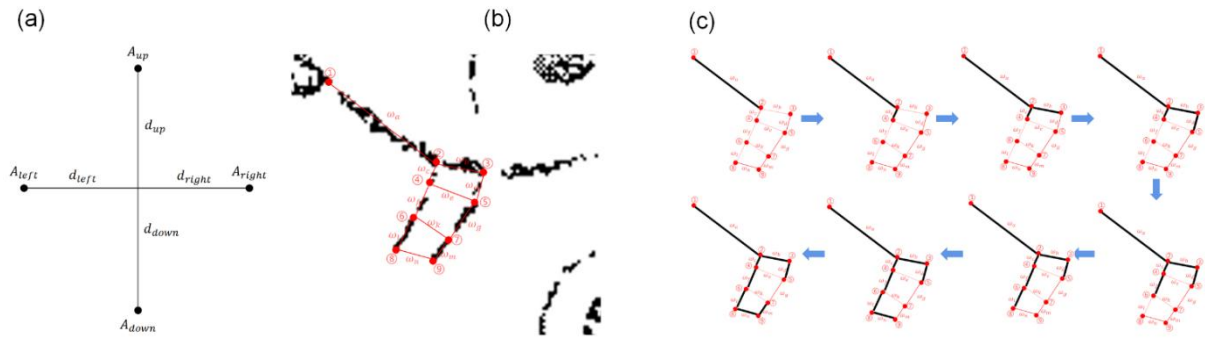


Figure 4 Schematic diagram. (a) Relationship between nodes and neighboring nodes, (b) Undirected connection illustration, (c) Processing legend of Minimum Spanning Tree based on Prim algorithm

4.3.3 Building a Cluster Hierarchy

Hierarchical structure organizes components via distance-sorted tree edges, forming a fully merged cluster with ambiguous inter-cluster boundaries. Elements are stored in an array, with edges represented by child-to-parent pointers (Figure 5(a)). Each node corresponds to a sample subset, with the root containing all points. Splitting begins at the top, iteratively removing the longest edge. Horizontal pruning treats low-density clusters as noise and is segmented to refine the boundaries.

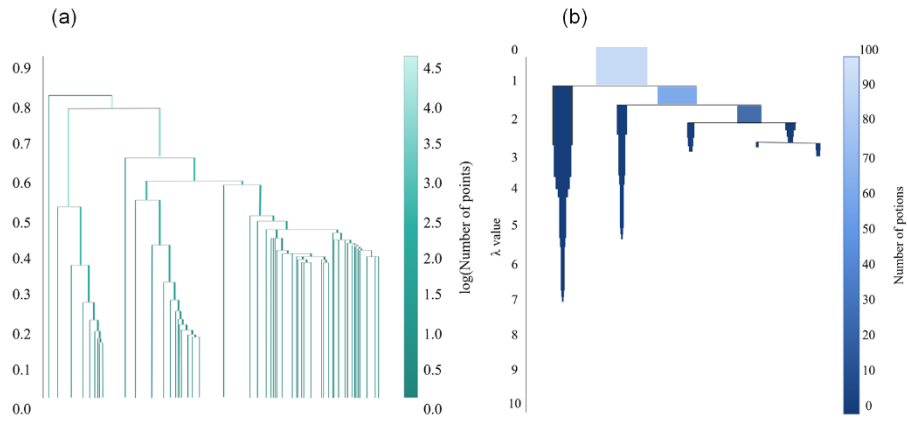


Figure 5 Legend of hierarchical clustering structure, (b) Compressed clustering tree

4.3.4 Cluster Hierarchy Compression

Minimum family size defines the smallest allowable cluster size. The clustering tree is traversed top-down, pruning nodes where either child subset contains fewer than M samples. If one subset is valid, the parent node's identity is retained; if both are invalid, the node is deleted. The resulting condensed tree exhibits fewer nodes (Figure. 5(b)), with line width indicating cluster density and node width decaying upward. Stability λ is quantified as the reciprocal of distance.

4.3.5 Stable Cluster Extraction

After compression, the tree graph contains no sparse points. Clusters are connected by iteratively merging the two closest clusters. Each node in the tree is characterized by two values: 1) λ_{birth} : Reciprocal of the cut edge length when splitting to generate the current node; 2) λ_{death} : Reciprocal of the broken edge length when the current node splits into subnodes, $\lambda_{birth} < \lambda_{death}$. For a sample point, a value λ_{A_i} is assigned, representing the reciprocal of the broken edge when leaving the node. After node splitting, a scatter point is located in a subset of samples smaller than the minimum cluster size and $\lambda_{birth} < \lambda_{A_i} < \lambda_{death}$. In normal splits, A_i transitions to a child node, $\lambda_{birth} = \lambda_{A_i} = \lambda_{death}$. Node stability $cluster_{A_i} = \sum_{p \in cluster} (\lambda_{A_i} - \lambda_{birth})$, $cluster_{A_i} < 0$ quantifies scattered points within a cluster, with higher stability indicating fewer outliers. Clustering proceeds via reverse topological traversal, initializing leaf nodes as clusters. The stability of the k th node updates to $cluster_{A_k} = cluster_{A_i}$ if the stability is less than the sum of its sub-cluster's stabilities. Candidate clusters are marked when parent stability exceeds the sum of child stabilities $cluster_{A_k}$. The root node yields the final planar clusters, illustrated in Figure 5(b). Membership strength is normalized by the distance from the cluster centre, where higher indicates proximity to the centroid. Cluster visualization uses colour intensity to represent normalized values.

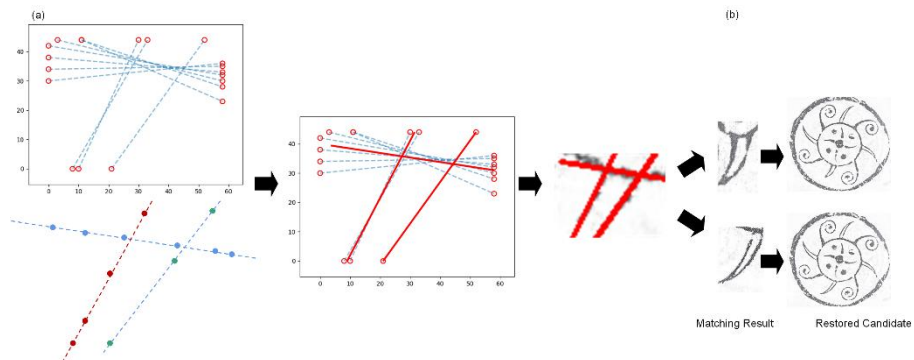


Figure 6 Candidate after geometric feature extraction and matching

Figure 6 shows geometric feature extraction and matching results. The database then identifies and traverses geometric relationships between straight lines, resulting in multiple matches.

4. Experiment and result

5.1 Dataset

A self-constructed image dataset of eaves tiles is used, including almost 500 images of those with symmetrical and repetitive compositions. Four hundred images were classified as training datasets, while 90 were classified as holdout datasets.

5.2 Experiment environment

Python 3.8 is the development programming language. The model training process utilized an NVIDIA GeForce 3090 GPU and a 12th Gen Intel Core i9-12900 CPU. The Adam optimizer is utilized in the training process with a learning rate of 0.0002, a batch size of 8, and a maximum iteration of 10000.

5.3 Baseline

Since the LaMa has a wide receptive field in images without perceptual loss, which is superior to the current state-of-the-art in complex scenarios, the author selected it to restore eaves tiles.

5.4 Criteria and Metric

5.4.1 Subjective qualitative criteria

Quality assessment criteria comprise: 1) completeness – the extent of essential visual information retention (features, textures, colours); 2) similitude – fidelity to the original object in form, structure, and chromatic attributes; 3) harmony – aesthetic coherence of compositional elements (colour, texture, layout); 4) symmetry – balanced spatial distribution of visual components.

5.4.2 Image processing related metrics

Key image processing metrics include: Fréchet Inception Distance (FID), which quantifying realism via Inception-v3 feature distributions; Differentiable Image Saliency Transform (DISTS), assessing perceptual quality through saliency modelling; L0-Structural Similarity Index (LOSSIM), combining SSIM and L0-norm for structural fidelity; and Single Inpainting Duration, measuring per-image computational efficiency. Lower FID and higher DISTS/LOSSIM values indicate superior performance.

5.5 Comparative experiment

HT_HDBSCAN and the Lama algorithm tested 90 tile rubbings with random damage. Figure 7 shows partial input and output.

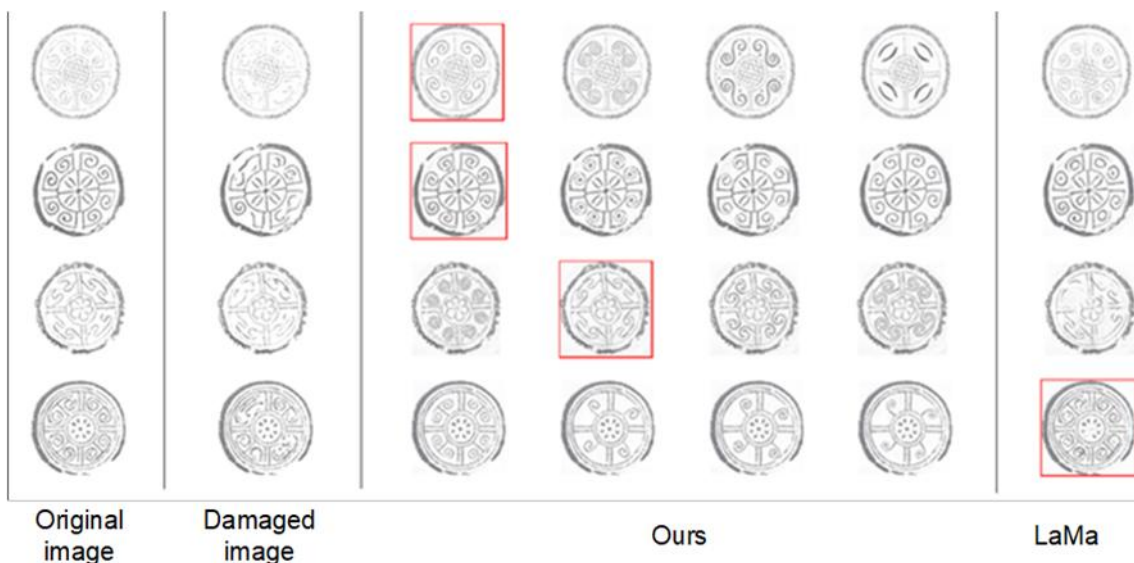


Figure 7 Comparison diagram of generated images through proposed framework and LaMa algorithm

Each input has multiple candidate outputs that satisfy clustering requirements; the red boxes indicate the best one selected by professionals based on other requirements, such as aesthetics, precision, reliability, and so on.

5. Discussion

6.1 Aesthetic evaluation based on high-frequency statistics

Using a 5-point Likert scale, the author evaluates image quality among 200 participants by creating a survey questionnaire using four subjective qualitative criteria.

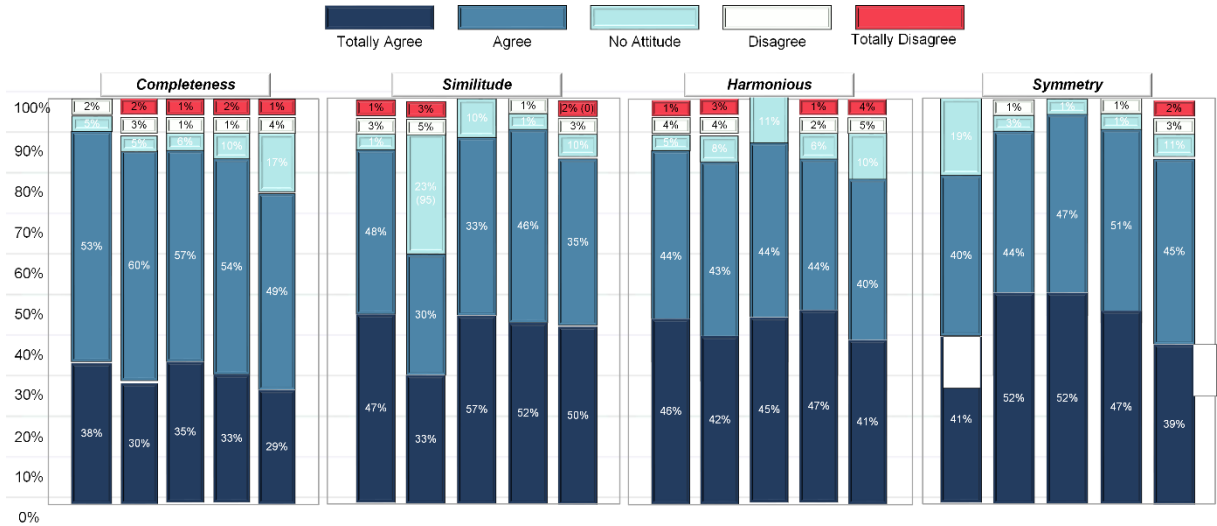


Figure 8 Frequency statistics diagram with different color blocks

The proposed model generates the first four columns, while LaMa generates the fifth. Figure 8 shows a positive attitude toward multi-criteria analysis, ranging from 81% to 98%. There is only a 78% to 85% attention rate for LaMa's image. Completion and symmetry also differ widely, with average values of 90.5%, 78%, 93.5%, and 84%, respectively. LaMa struggles to align pixels with subtle colour changes and predominantly geometric lines regarding intricate building details. As aesthetic judgments are subjective, there is rarely a relationship between aesthetic judgments and generated images.

6.2 Statistical analysis

As shown in Table 1, the proposed framework's FID is lower, indicating a more authentic generated image. Our method's ability to learn the original image's distribution and generate features significantly raises DISTS values compared to LaMa. Compared to LaMa, our LOSSIM value is 0.8513, indicating greater similarity. This method demonstrates excellent computational efficiency and real-time performance, with a recovery time of $5.59e^{-2}$ seconds, three times faster than LaMa.

Table 1 The different criteria aim to proposed framework and LaMa

Metric	FID↓	DISTS↓	LOSSIM↓	Single inpainting duration(second)↓
Ours	27.25	0.2135	0.8513	$5.59e^{-2}$
LaMa	35.85	0.3513	0.8925	19.79

6.3 Limitation

Excellent metrics verify the generated image's visual perception, fairness and bias, predictive ability, and interpretability. Nevertheless, many areas need improvement. After generating multiple images, further evaluation is needed to reduce confusion. Besides, geometric feature items in the Image Feature Database cannot cover all eaves tiles, which may limit the application scope of this framework. Therefore, extending item features and creating a transparent classification system is necessary.

6. Conclusion

Current methods lack specialized solutions for damaged architectural ornaments like eaves tiles. This study proposes a heuristic deep learning framework trained on a custom dataset to enhance geometric feature-based restoration, called Staged Refined Restoration Framework for Architectural Heritage Damaged Eaves Tiles. Leveraging a pre-established unitized database, it bypasses reliance on historical sources, employing subject-specific networks to restore damaged patterns. The framework outperforms conventional inpainting techniques by integrating the Minimum Spanning Tree and automating parameter transfer, enabling intricate structural recovery. Experiments confirm superior restoration accuracy and relevance, offering multiple style-compliant candidates. While adaptable to similar ornaments (e.g., bas-reliefs, cornices), limitations persist: geometric consistency alone cannot ensure aesthetic cohesion. Future work requires automated damage detection, candidate filtering, and database expansion incorporating multi-dimensional metrics for holistic heritage restoration.

Acknowledgements

Support for this study is provided by the National Key R&D Program of China (No. 2022YFC3802201) and the National Natural Science Foundation of China (Grant No. U21A20151).

Reference

- [1] B. Yildizlar, B. Sayin, and C. Akcay, "A Case Study on the Restoration of A Historical Masonry Building Based on Field Studies and Laboratory Analyses," *International Journal of Architectural Heritage*, vol. 14, no. 9, pp. 1341-1359, Oct 2020, doi:10.1080/15583058.2019.1607625
- [2] J. Owen, "The Grammar of Ornament," 1910, the referenced item does not yet have a DOI number
- [3] C. A. Evans, P. J. Coombes, and R. H. Dunstan, "Wind, rain and bacteria: The effect of weather on the microbial composition of roof-harvested rainwater," *Water Research*, vol. 40, no. 1, pp. 37-44, 2006, doi:10.1016/j.watres.2005.10.034
- [4] Q. Lu, L. Wang, X. Meng, W. J. J. F. S. Y. T. X. J. o. C.-A. D. Wang, and C. Graphics, "The Bas-Relief Generation Method of Human Faces from 3D Depth Images and 2D Intensity Images," vol. 27, no. 7, pp. 1172-1181, 2015, the referenced item does not yet have a DOI number:
- [5] J. Shang, M. J. C. a. Wang, and v. worlds, "Variety decorative bas-relief generation based on normal prediction and transfer," no. 3/4, p. 33, 2022, doi:10.1002/cav.2068
- [6] A. Pesenti, L. Cozzi, and C. Elliott, "Apparitions: Frottages and Rubbings from 1860 to Now," 2015, the referenced item does not yet have a DOI number
- [7] Morkunaite, Bausys, and Zavadskas, "Contractor Selection for Sgraffito Decoration of Cultural Heritage Buildings Using the WASPAS-SVNS Method," *Sustainability*, vol. 11, no. 22, p. 6444, 2019, doi:10.3390/su11226444
- [8] G. Aktürk, "Remembering traditional craftsmanship: conserving a heritage of woodworking in Rize, Turkey," *International Journal of Intangible Heritage*, vol. 15, pp. 134-146, 2020, doi:10.35638/IJIH.2020.15.2.009
- [9] Jun, Yan, Xiaoxian, and Shan, "Research on the Application of Traditional Decorative Elements in Contemporary Architectural Design," in *International Conference on Humanities Science and Society Development*, 2017, doi:10.2991/ichssd-17.2018.72.
- [10] I. C. C. Camacho and K. Wang, "A Comprehensive Review of Deep-Learning-Based Methods for Image Forensics," *Journal of Imaging*, vol. 7, no. 4, p. 69, the referenced item does not yet have a DOI number
- [11] M. Bertalmio, G. Sapiro, V. Caselles, and C. Ballester, "Image inpainting," in *Proceedings of the 27th annual conference on Computer graphics and interactive techniques*, 2000, pp. 417-424, the referenced item does not yet have a DOI number
- [12] J. C. Hung, C.-H. Huang, Y.-C. Liao, N. C. Tang, and T.-J. J. J. S. Chen, "Exemplar-based Image Inpainting base on Structure Construction," vol. 3, no. 8, pp. 57-64, 2008, doi:10.4304/jsw.3.8.57-64
- [13] A. J. J. o. g. t. Telea, "An image inpainting technique based on the fast marching method," vol. 9, no. 1, pp. 23-34, 2004, the referenced item does not yet have a DOI number
- [14] B. R. Mohapatra, A. Mishra, and S. K. J. I. J. o. r. i. a. t. Rout, "A comprehensive review on image restoration techniques," vol. 2, no. 3, pp. 101-105, 2014, doi:10.1080/15583058.2019.1607625